Bulletin of Mathematical Biology Vol. 53, No. 3, pp. 425–441, 1991.
Printed in Great Britain.

0092-8240/91$3.00 + 0.00
Pergamon Press plc

ON THE STRUCTURE OF THE AERIAL VISUAL FIELD OF AQUATIC ANIMALS DISTORTED BY REFRACTION

■ GÁBOR HORVÁTH
Central Research Institute for Physics of the Hungarian Academy of Sciences,
Biophysical Group,
H-1525 Budapest, POB 49, Hungary

■ DEZSÖ VARJÚ
Lehrstuhl für Biokybernetik,
Universität Tübingen,
Auf der Morgenstelle 28, D-7400 Tübingen 1, F.R.G.

The aerial visual field of aquatic animals living near the water surface is distorted by refraction. The imaging of aerial objects by one or two submerged eyes is studied. The aerial binocular image field is determined for pairs of submerged eyes in horizonal and vertical planes. These two image spaces have significantly different structures. Aquatic animals have to correct for refraction, adapting themselves to the former aerial image field in order to recognize aerial predators or to capture such prey. The other aerial image space is only of theoretical interest.

1. Introduction. It is a well-known phenomenon that the apparent position of an aerial object when viewed from underwater does not coincide with its true position due to the refraction of light at the water surface. This distortion can be experienced in everyday life when, for example, a diver views the aerial world (Harmon and Cline, 1980; Walker, 1984).

Coping with the problem of refraction is of particular importance for amphibians when they are submerged and for aquatic animals living near the water surface whenever they have to capture aerial prey or recognize aerial predators (Curio, 1976; Schusterman, 1981). It is not all the same to a seal, for example on emerging from the water, whether one of its companions waits for it on the edge of an ice-hole, or its main predator, a polar bear. In the escape strategy of an emerging seal attacked by a polar bear, the structure of its aerial visual field can play a primary role in considering the apparent and true position of its aerial predator (Schusterman, 1981). In the reverse case, when a seal lies on the edge of an ice-hole and watches the underwater world, for example, some possible bio-optical consequences to the seal's visual detection of underwater prey and predator have been discussed by the authors elsewhere (Horváth and Varjú, 1990).

In spite of the fact that the number of animals which must take into account

the distortion of their visual field due to refraction is large, it has only been proven with one non-aquatic and one aquatic animal that correction for refraction occurs. The non-aquatic animal is a western reef heron, *Egretta gularis schistacea* (Katzir and Intrator, 1987), the aquatic animal is the archerfish *Toxotes*.

The archerfish spits droplets of water at aerial insects, knocking them onto the water. Since the fish's eyes remain below the water surface during sighting and spitting, it must deal with potentially severe refraction effects at the air–water interface. The ability to cope with refraction has been demonstrated up to now in two species of archerfish. *Toxotes jaculatrix* positions itself directly beneath its prey prior to spitting, and thus avoids refraction (Lüling, 1963; Bekoff and Dorr, 1976). However, *Toxotes chatareus* does not spit from a position directly below the prey, but can correctly set its spitting angle to compensate for the refraction unique to a variety of positions (Dill, 1977). The fish can correct for large refraction effects on the prey's apparent elevation or apparent height. However, spitting accuracy decreases with increasing height or distance of the prey. *Toxotes chatareus* also corrects for the curvature of the water droplet's trajectory. Since spitting velocity is relatively constant, the fish makes this correction via its spitting angle.

The aerial visual field distorted by refraction for the above aquatic animals and amphibians, and their astigmatic imaging of aerial objects viewed by one or two submerged eyes have not been yet theoretically or geometric optically studied. These are treated in this work. The similarly interesting reverse problem when underwater objects are viewed from the air is treated elsewhere (Horváth and Varjú, 1990).

2. Imaging of Aerial Objects with One Submerged Eye. Consider an aerial object point O in the system of co-ordinates of Fig. 1. From O a bundle of rays of light with aperture 2π steradians is radiated towards the water surface. The evolute (surface with cylindrical symmetry) of the refracted rays extrapolated backwards, its main section and the area bounded by this evolute is called caustic, caustic curve and image area (IA), respectively. In the IA intersect the refracted rays are extrapolated backwards.

In every point of the IA without its axis (coinciding with the y-axis) two refracted rays extrapolated backwards intersect in the same vertical plane (see point D in Fig. 1, for example). In a point of the axis of the IA intersect those refracted rays, extrapolated backwards, form a cone (see the point B in Fig. 1, for example).

Consider that homocentric slender bundle of rays which originates in the aerial point O on the y-axis and passes through the pupil of the eye of an aquatic animal (Fig. 2). When this bundle is incident at the water surface, it is refracted into a system of rays that is not homocentric; an astigmatic bundle of

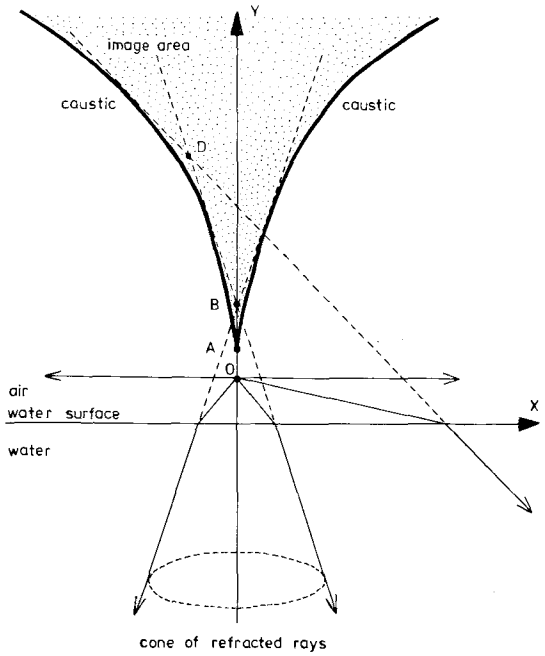

Figure 1. An aerial bundle of rays of light starting from O with aperture 2π steradians, the evolute called caustic of the refracted rays extrapolated backwards, and the image area (dotted).

refracted rays is obtained. Figure 2 represents the main section of this astigmatic refracted pupil bundle. The boundary rays extrapolated backwards of the refracted pupil bundle cut a body from the IA. This slender wedge-shaped body is called astigmatic image body (AIB) of the object point O, and it can be seen in Fig. 3. The edge is a line segment I_1I_3 on the axis, the back is an area $C_1C_4C_3C_5$ on the caustic surface. In every point of the AIB without its edge I_1I_3 two refracted rays extrapolated backwards intersect, therefore two rays of light construct the image of these points on the retina.

A cone of refracted rays crosses the pupil in an arc (see the arc $S_4S_2S_5$ in Fig. 2, for example). The rays extrapolated backwards passing through a pupil arc intersect in a point of the edge I_1I_3, therefore a large number of rays construct the image of every edge point of the AIB on the retina. The longest pupil arc $S_4S_2S_5$ passes through the centre S_2 of the pupil, and the length of the pupil arcs decreases as the arc moves off from S_2.

The light intensity of an image point is proportional to the number of the constructing rays. Therefore the brightest part of the AIB is its edge I_1I_3, the brightest point of this edge is I_2, belonging to the pupil arc $S_4S_2S_5$. The brightness of the edge points decreases towards the end points I_1 and I_3. The intensity i_{min} of the points of the AIB is low in comparison with that of its edge

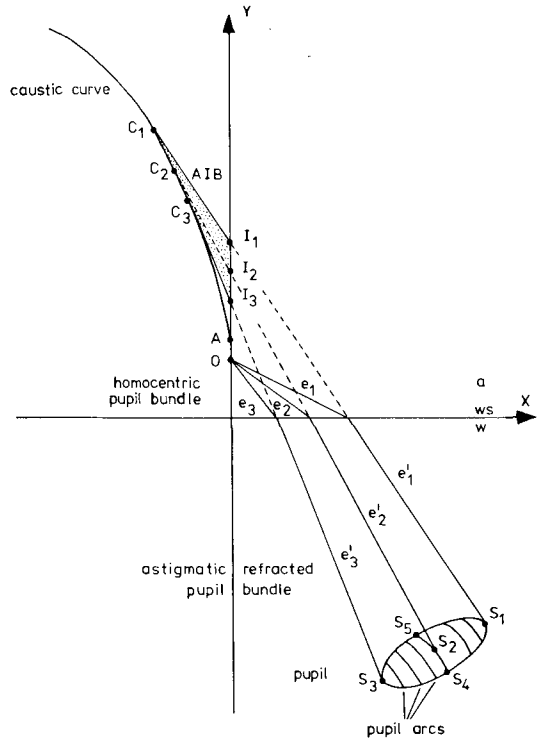

Figure 2. The main section of the aerial homocentric and the submerged astigmatic refracted pupil bundle passing through the pupil of the lens eye of an aquatic animal. a: air, ws: water surface, w: water, AIB: astigmatic image body (dotted).

I_1I_3. Two very small elementary bundles of rays contribute to i_{min}, which are incident on two visual cells of the retina. The intensity of an edge point of the AIB is proportional to the length l of the pupil arc belonging to this point weighed by the number N of the visual cells on the retina along this arc. Provided that the density of the receptor cells is homogeneous, the intensity of an edge point is therefore

$$i = i_{min} l / l_{min}, \tag{1}$$

where l_{min} belongs to a single visual cell. If the intensity of the brightest edge point I_2 is i_{max}, and the length of the pupil arc $S_4S_2S_5$ belonging to I_2 is l_{max}, then the intensity of an edge point can be expressed also by

$$i = i_{max} l / l_{max}. \tag{2}$$

Figure 4a shows the shape of the AIB in the case of a near circular pupil, when $\overline{S_4S_5} \approx \overline{S_1S_3}$. The AIB is vertically and horizonally flattened on its edge and back, respectively. (In Fig. 4 only the visible part of the boundary surface

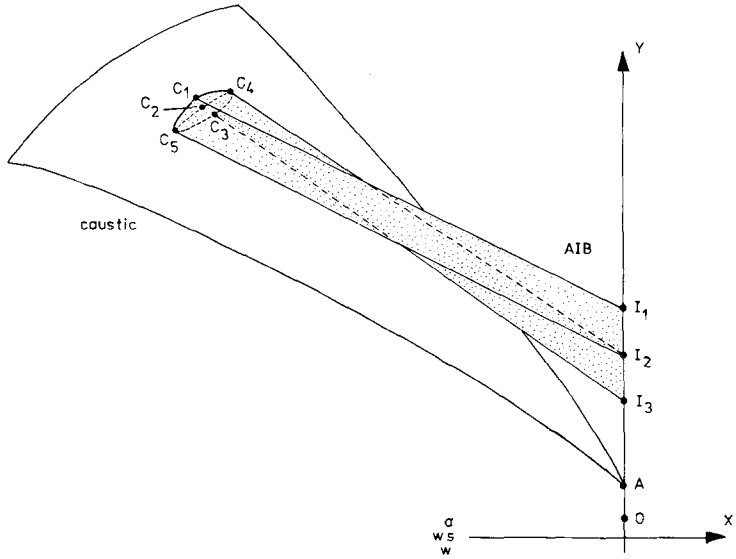

Figure 3. The wedge-shaped astigmatic image body (AIB, dotted) is the astigmatic image of the aerial object point O. The AIB is obtained by extrapolating backwards the rays in the astigmatic refracted pupil bundle.

of the AIB is represented). In Fig. 4b the shape of the AIB can be seen for a vertically elongated pupil ($\overline{S_4S_5} \ll \overline{S_1S_3}$). In this case almost the whole AIB is flattened in the vertical plane; it has a very narrow horizontally flattened back, and it can be approximated by the triangle $I_1I_3C_1$ in the limit $\overline{S_4S_5} \to 0$. When the pupil is horizontally elongated ($\overline{S_4S_5} \gg \overline{S_1S_3}$), almost the whole AIB is flattened in the plane $I_2C_4C_5$; its vertically flattened edge part is very slender. Then the AIB can be approximated by the triangle $I_2C_4C_5$ in the limit $\overline{S_1S_3} \to 0$.

Consider the intensity of the edge points for the above three AIB as a function of $q = 2v/\overline{S_1S_3}$, where v is the vertical distance between the investigated pupil arc with length $l(q)$ and the centre S_2 of the pupil. The function $l(q)/l_{max}$ decreases rapidly from 1 to zero as q increases from zero to 1 in the case of Fig. 4c. This decrease is slower in the case of Fig. 4a, and slowest in the case of Fig. 4b; only near the points S_1 and S_3 does it become steep.

Using equation (2), it can be seen that in the case of the horizontally elongated pupil, the edge point I_2 and its very small surroundings on the edge, are bright in comparison with the other edge points. When the pupil is near circular, the highlighted surroundings of I_2 are larger, and extend almost to the whole edge in case of the vertically elongated pupil.

Using equation (1), we can compare the intensity of the highlighted edge part to that of the other points of the AIB. The quotient $l/l_{min} = i/i_{min}$ is large for the highlighted edge part in the case of the horizontally elongated and the near circular pupil, but it is small for a vertically elongated narrow pupil.

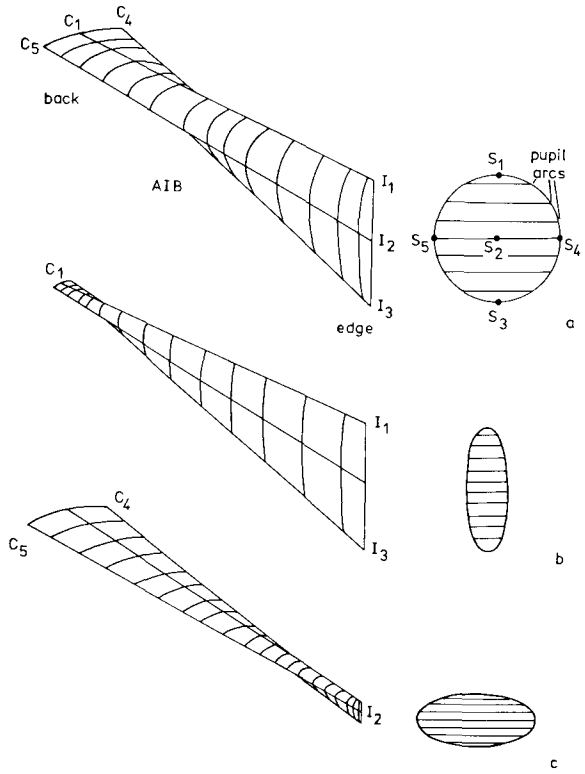

Figure 4. The shape of the AIB for a near circular (a), a vertically (b) and a horizontally (c) elongated pupil.

3. Binocular Imaging of Aerial Objects. In general the diameter of the pupil can be neglected in comparison with the distance between the eye of an aquatic animal and an aerial object viewed by it. Therefore the AIB is very slender, and it can be approximated by the astigmatic image line $\overline{IC}$ which extends from the edge (I) towards the back (C).

Binocular vision results in at least two definite, unique positions. If a small object is observed with the eyes along a horizontal line, the two narrow bundles of rays entering the eyes appear to come from I (Fig. 5a), but if the eyes lie on a vertical line, the two narrow bundles of rays appear to come from C (Fig. 5b).

If the eyes lie in a horizontal plane (parallel to the water surface), the binocular image of the aerial object point O lies at the coinciding points I_R and I_L for the right and left eyes, respectively (Fig. 5a). If the eyes and the object point lie in a vertical plane, the binocular image lies at the coinciding points C_R and C_L for the right and left eyes, respectively (Fig. 5b). In any other case there is no binocular image point, because the two bundles of rays entering the eyes do not intersect; that is to say, the astigmatic image lines of the right and left

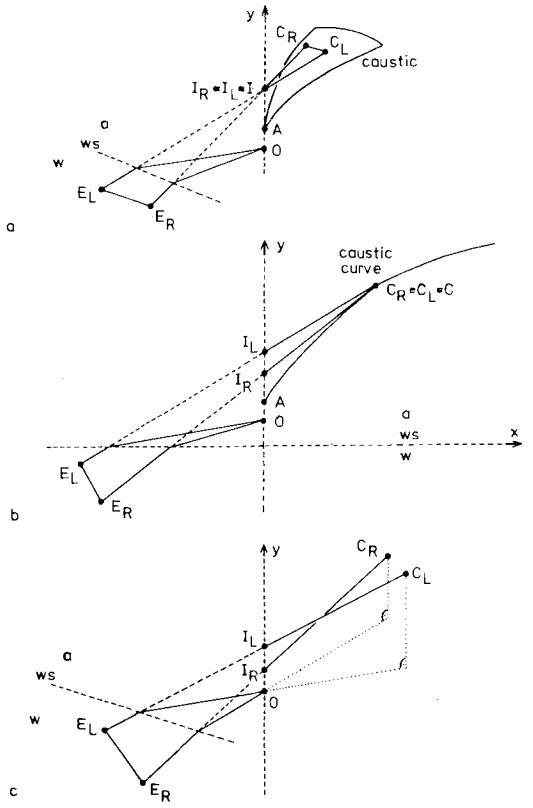

Figure 5. (a) When the right and left eyes E_R and E_L of an aquatic animal lie in a horizontal plane, the astigmatic image lines $\overline{I_R C_R}$ and $\overline{I_L C_L}$ intersect in the point $I_R \equiv I_L \equiv I$, so that the binocular ordinary image point of O is I. (b) If the eyes and the object point O lie in the same vertical plane, the astigmatic image lines intersect in the point $C_R \equiv C_L \equiv C$. Therefore the binocular extraordinary image point of O is C. (c) In any other case the astigmatic image lines have no common point, and there is no binocular image point.

eyes have no common point (Fig. 5c). Binocular depth perception is, therefore, not possible, only the direction of an object point can be perceived by submerged eyes.

Since objects are usually observed with both eyes lying in a horizontal plane, the ordinary binocular image point of an aerial object point O is I. The customary image of the aerial world is determined by these points I, and it is called aerial binocular ordinary image field (ABOIF) in this work. The space determined by the points C is called aerial binocular extraordinary image field (ABEIF). It is the binocular image of the aerial world if the eyes line on a vertical line. Further on in this work we determine the caustic curve, the ABOIF and the ABEIF for a grid of aerial object points.

4. The Caustic Curve. The caustic curve is determined by the extraordinary image points C of an aerial object point. Let two rays of e_1 and e_2 originate in a vertical plane in the aerial object point $\underline{O}=(0, H)$. The angles between the water surface and the refracted rays e_1' and e_2' are α and $\alpha+\Delta\alpha$, respectively. The extraordinary image point $C(x, y)$ of O is determined by the intersection of the lines e_1' and e_2' extrapolated backwards as $\Delta\alpha\to 0$. The equation of the line e_1' in the system of co-ordinates of Fig. 1 is

$$y_1(x)=-(x-H \operatorname{tg}\beta)\operatorname{tg}\alpha \tag{3}$$

where H is the distance between the water surface and the point O; β is the angle between the axis y and the line e_1. On the basis of the refraction law

$$\frac{\sin\beta}{\cos\alpha}=n, \qquad \operatorname{tg}\beta=\frac{n\cos\alpha}{[1-n^2\cos^2\alpha]^{1/2}}. \tag{4}$$

From equations (3) and (4) we obtain

$$y_1(x)=-\left[x-\frac{Hn\cos\alpha}{[1-n^2\cos^2\alpha]^{1/2}}\right]\operatorname{tg}\alpha. \tag{5}$$

Similarly the equation of the line e_2' can be obtained as

$$y_2(x)=-\left[x-\frac{Hn\cos(\alpha+\Delta\alpha)}{[1-n^2\cos^2(\alpha+\Delta\alpha)]^{1/2}}\right]\operatorname{tg}(\alpha+\Delta\alpha). \tag{6}$$

In general the diameter of the pupil can be neglected in comparison to the distance between the eye and the object point, and therefore $\Delta\alpha\ll 1$. Thus the following approximation can be used

$$\operatorname{tg}(\alpha+\Delta\alpha)\approx\frac{\operatorname{tg}\alpha+\Delta\alpha}{1-\Delta\alpha\operatorname{tg}\alpha}, \qquad \cos(\alpha+\Delta\alpha)\approx\cos\alpha-\Delta\alpha\sin\alpha. \tag{7}$$

The co-ordinates x, y of the point C are determined by the equation

$$y_1(x)=y_2(x) \quad \text{as} \quad \Delta\alpha\to 0. \tag{8}$$

From equations (5–8) we obtain for the abscissa x of C

$$x=Hn\cos^2\alpha\lim_{\Delta\alpha\to 0}\left[\frac{\dfrac{(\operatorname{tg}\alpha+\Delta\alpha)(\cos\alpha-\Delta\alpha\sin\alpha)}{[1-n^2(\cos\alpha-\Delta\alpha\sin\alpha)^2]^{1/2}}-\dfrac{\sin\alpha(1-\Delta\alpha\operatorname{tg}\alpha)}{[1-n^2\cos^2\alpha]^{1/2}}}{\Delta\alpha}\right]. \tag{9}$$

Using the L'Hospital law, making the limit $\Delta\alpha\to 0$, we obtain from equations (5) and (9) the co-ordinates of C as a function of the angle α

$$x(\alpha)=-\frac{Hn(n^2-1)\cos^3\alpha}{[1-n^2\cos^2\alpha]^{3/2}},\quad y(\alpha)=\frac{Hn\sin^3\alpha}{[1-n^2\cos^2\alpha]^{3/2}}. \tag{10}$$

Eliminating the angle α from equation (10), we obtain the function $y_c(x)$ of the caustic curve

$$y_c(x)=Hn\left[1+(n^2-1)^{1/3}\left(\frac{x}{nH}\right)^{2/3}\right]^{3/2}. \tag{11}$$

The co-ordinates of the peak point A of the caustic are

$$\underline{A}=(O,\ Hn). \tag{12}$$

From equation (10) we deduce that the extraordinary image point C moves along the caustic curve from the point A towards infinity, as α decreases from $\pi/2$ to zero.

Since the caustic is the evolute of the refracted rays extrapolated backwards, the abscissa x can be determined from the disappearance of the partial differential quotient $\partial y_1/\partial\alpha$, too. From equation (5)

$$\frac{\partial y_1}{\partial\alpha}=-\frac{x}{\cos^2\alpha}-\frac{Hn(n^2-1)\cos\alpha}{(1-n^2\cos^2\alpha)^{3/2}}=0 \tag{13}$$

follows, and from equation (13) the same expression as in equation (10) can be derived.

5. The Aerial Binocular Ordinary Image Field (ABOIF). Consider an aerial object point $O(x, y)$ observed by an aquatic animal with eyes placed in a horizontal plane in the system of co-ordinates of Fig. 6. The binocular ordinary image of $O(x, y)$ is the point $I(x, y')$. If a ray e starting from O reaches the eye E of the animal after refraction (e'), I lies in the intersection of the line e' extrapolated backwards and the vertical line passing through O, as we have seen above.

Let the eyes of the animal be on the axis y at distance L from the water surface. We can write on the basis of Fig. 6

$$L\operatorname{ctg}\alpha+y\operatorname{tg}\beta=x,\qquad y'=x\operatorname{tg}\alpha-L. \tag{14}$$

From equations (4) and (14) we obtain

$$\begin{aligned}&F(\operatorname{tg}\alpha)=a_0+a_1\operatorname{tg}\alpha+a_2\operatorname{tg}^2\alpha+a_3\operatorname{tg}^3\alpha+a_4\operatorname{tg}^4\alpha=0,\\&a_0=-L^2(n^2-1),\ a_1=2Lx(n^2-1),\ a_2=L^2+x^2-n^2(x^2+y^2),\\&a_3=-2Lx,\ a_4=x^2.\end{aligned} \tag{15}$$

The fourth degree equation (15) can be solved analytically for tg α. However,

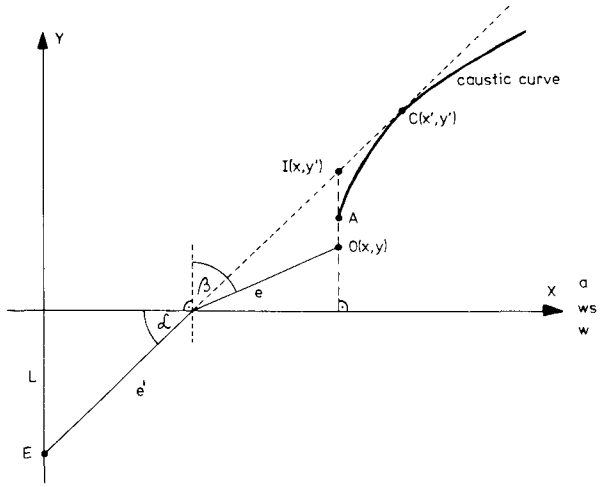

Figure 6. Determination of the aerial binocular ordinary and extraordinary image field (ABOIF and ABEIF). The binocular ordinary and extraordinary image of O is I and C, respectively; the eyes of an aquatic animal are on the y axis at distance L from the water surface.

because of the complexity it is more expedient to solve it numerically, using the tangent method of Newton, for example. The following recursion

$$(\text{tg}\ \alpha)_{i+1} = (\text{tg}\ \alpha)_i - \frac{F[(\text{tg}\ \alpha)_i]}{\dot{F}[(\text{tg}\ \alpha)_i]}, \qquad \dot{F} \equiv \frac{\mathrm{d}F}{\mathrm{d}(\text{tg}\ \alpha)} \tag{16}$$

yields the approximate roots $(\text{tg}\ \alpha)_i$. Solving equation (15) for tg α numerically, the ordinate y' of the ordinary image point I can be obtained from equation (14).

After these we can determine the ABOIF distorted by refraction for an aquatic animal. Consider the two-dimensional vertically oriented quadratic grid in Fig. 7 as the aerial object space

$$y = iR, \qquad x = \pm jR; \qquad i, j = 0, 1, 2, 3 \ldots \tag{17}$$

where $R > 0$ is the grid parameter. The binocular ordinary images of the vertical lines $x = \pm jR$ are also vertical lines. From equations (14) and (15), the binocular ordinary images of the horizontal lines $y = iR$ can be determined numerically.

The results are shown in Fig. 8 for two different values of the relative grid parameter R/L. For a given value of R, and for the near-space ABOIF R/L is small, for the far-space it is large. From equations (11) and (14) the following limits

$$\lim_{x \to 0} y' = ny, \qquad \lim_{x \to \infty} y' = \infty \tag{18}$$

are obtained.

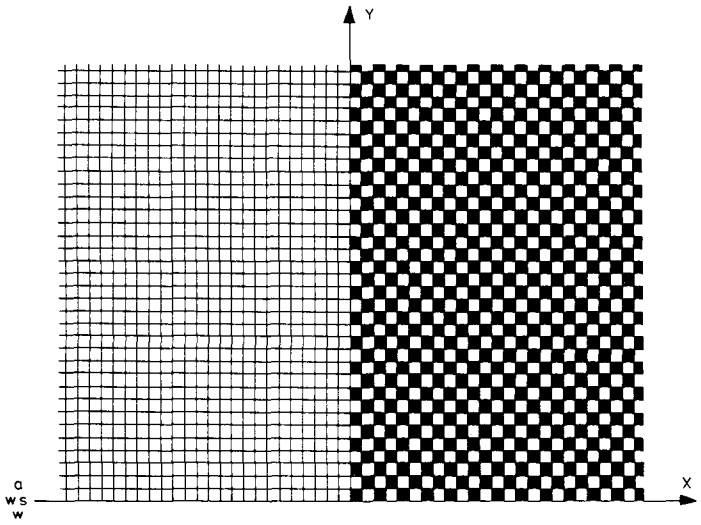

Figure 7. The two-dimensional quadratic grid with grid parameter R as the aerial object space. For the sake of a better visualization the cells are alternately coloured white and black on the right part of the object space.

6. The Aerial Binocular Extraordinary Image Field (ABEIF). The ABEIF is determined by the extraordinary image points $C(x', y')$ placed on the caustic. Using equation (10), we can write on the basis of Fig. 6

$$y' = y \frac{n \sin^3 \alpha}{(1 - n^2 \cos^2 \alpha)^{3/2}}, \tag{19}$$

$$x' = x + y \frac{n(n^2 - 1)\cos^3 \alpha}{(1 - n^2 \cos^2 \alpha)^{3/2}}, \tag{20}$$

$$L + y' = x' \operatorname{tg} \alpha. \tag{21}$$

We obtain from equations (19–21)

$$x'^3 - x' \frac{(L + y')^3}{(n^2 - 1)y'} + \frac{x(L + y')^3}{(n^2 - 1)y'} = 0. \tag{22}$$

Eliminating tg α from equations (19) and (21) results in

$$x'(y', y, L) = (L + y') \left(\frac{y}{n^2 y'} \right)^{1/3} \left[\frac{\left(\frac{n^2 y'}{y} \right)^{2/3} - n^2}{n^2 - 1} \right]^{1/2}. \tag{23}$$

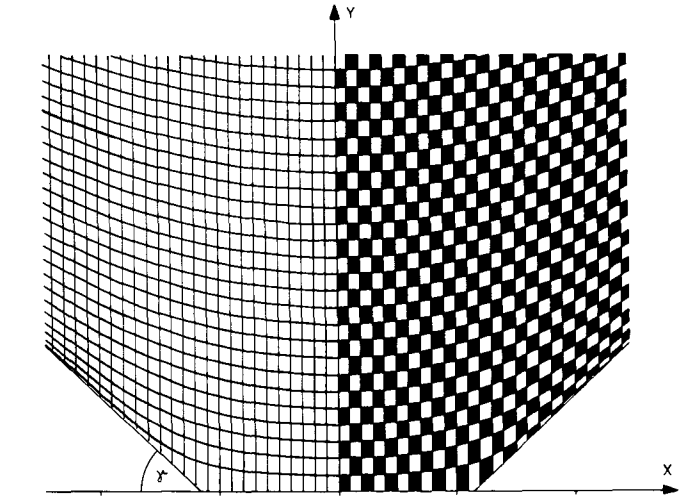

a

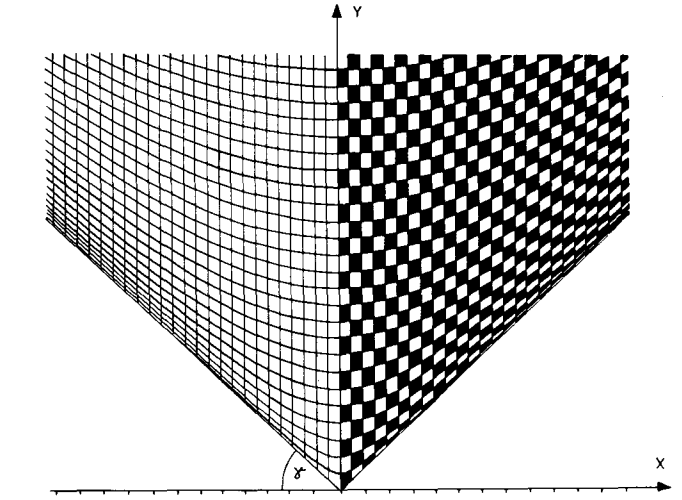

b

Figure 8. (a) The aerial binocular ordinary image field (ABOIF) with the relative grid parameter $R/L=0.1$ (near-space). The scale on the x axis is L which holds also for the y axis. (b) As (a) for the relative grid parameter $R/L=10$ (far-space). The scale on the x axis is $20L$. $\gamma=\arccos(1/n)$.

The function $x'(y', y, L)$ gives the binocular extraordinary image of the horizontal lines ($y = \text{constant} \geqslant 0$) of the aerial object field. With the Cardano-formula we obtain from equation (22)

$$x'(y', x, L) = \left[-\frac{Q}{2} + \left(\frac{Q^2}{4} + \frac{p^3}{27} \right)^{1/2} \right]^{1/3} + \left[-\frac{Q}{2} - \left(\frac{Q^2}{4} + \frac{p^3}{27} \right)^{1/2} \right]^{1/3},$$

$$p = -\frac{(L+y')^3}{(n^2-1)y'}, \qquad Q = -px. \tag{24}$$

The function $x'(y', x, L)$ gives the binocular extraordinary image of the vertical half lines ($x = \text{constant}$, $y \geqslant 0$) of the aerial object field.

The functions $x'(x, y)$ and $y'(x, y)$ cannot be determined analytically, so we use the functions (23) and (24), to calculate the near-space and the far-space of the ABEIF, which are shown in Fig. 9a and b, respectively. In Fig. 10 and 11 examples can be seen for the relation between the ABOIF and the ABEIF. The slanted lines between corresponding extraordinary and ordinary curves in Fig. 10 and 11 are the astigmatic image lines $\overline{IC}$.

7. Conclusions. An aerial object can be imaged by a single submerged lens eye, when the distances between the eye and the object are comparable to the diameter of the pupil (very near-space). The astigmatic imaging due to the refraction on the water surface can be characterized by the astigmatic image body (AIB) of an aerial object point. The shape of the AIB depends on the form of the pupil.

(i) When the pupil is horizontally elongated, the most highlighted part of the AIB is limited almost only to its edge point I_2, therefore the image of an aerial object point O is I_2 (Fig. 4c).

(ii) When the pupil is near circular, the most highlighted part of the AIB extends almost to its whole edge, the image of O is the line $\overline{I_1 I_3}$ (Fig. 4a).

The other points of the AIB play no role in the image construction in the case of a near circular or horizontally elongated pupil, since they are very dim. Except for its edge the AIB can be called the imperceptible astigmatic phantom image of O.

(iii) In the case of a vertically elongated, very narrow pupil, the most highlighted part of the AIB is its edge, but the difference between the brightness of its edge and that of its other points is little (Fig. 4b). Therefore the astigmatic phantom image (the AIB) is perceptible to a small degree, and it determines and characterizes the sharpness and the contrast of the very near-space imaging of aerial objects.

However, in general the distance between the two submerged eyes and the aerial object viewed by them is much larger than the diameter of the pupil. Then the binocular imaging becomes conspicuous. On the basis of Fig. 5, the

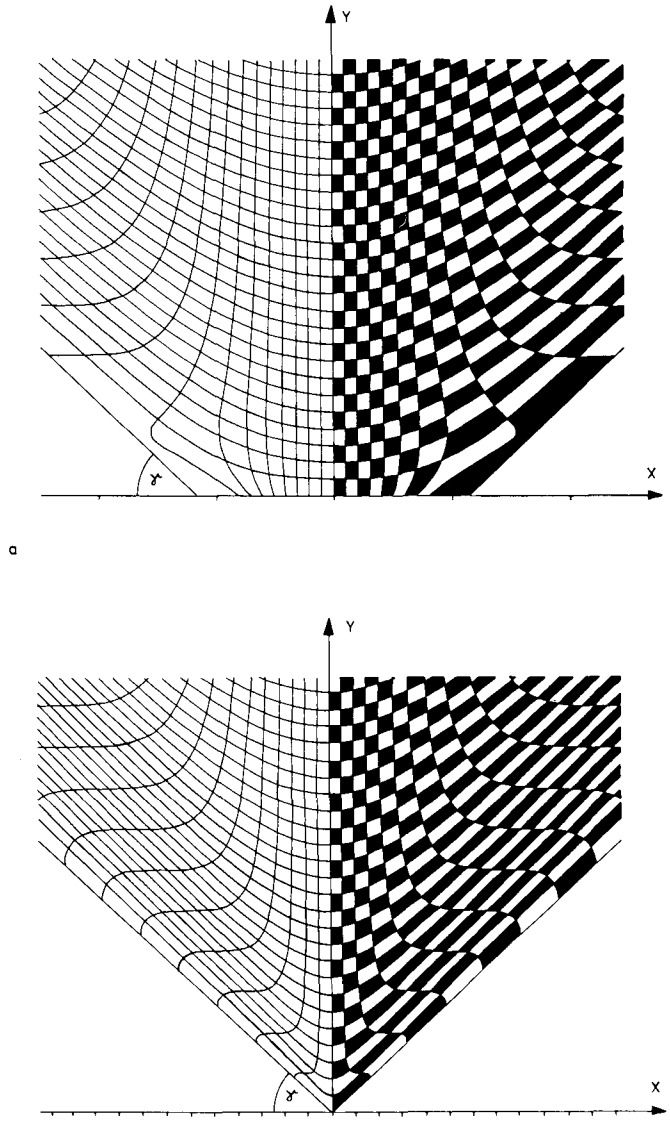

Figure 9. (a) The near-space of the aerial binocular extraordinary image field (ABEIF) for $R/L=0.1$. (b) The far-space of the ABEIF for $R/L=10$. Same scales as in Fig. 8.

following can be concluded for the aerial binocular visual field for differently arranged eyes of an aquatic animal.

(iv) When the eyes are placed along a vertical line (at right angles to the water surface) a vertical plane, in which both eyes lie, can pass through any aerial

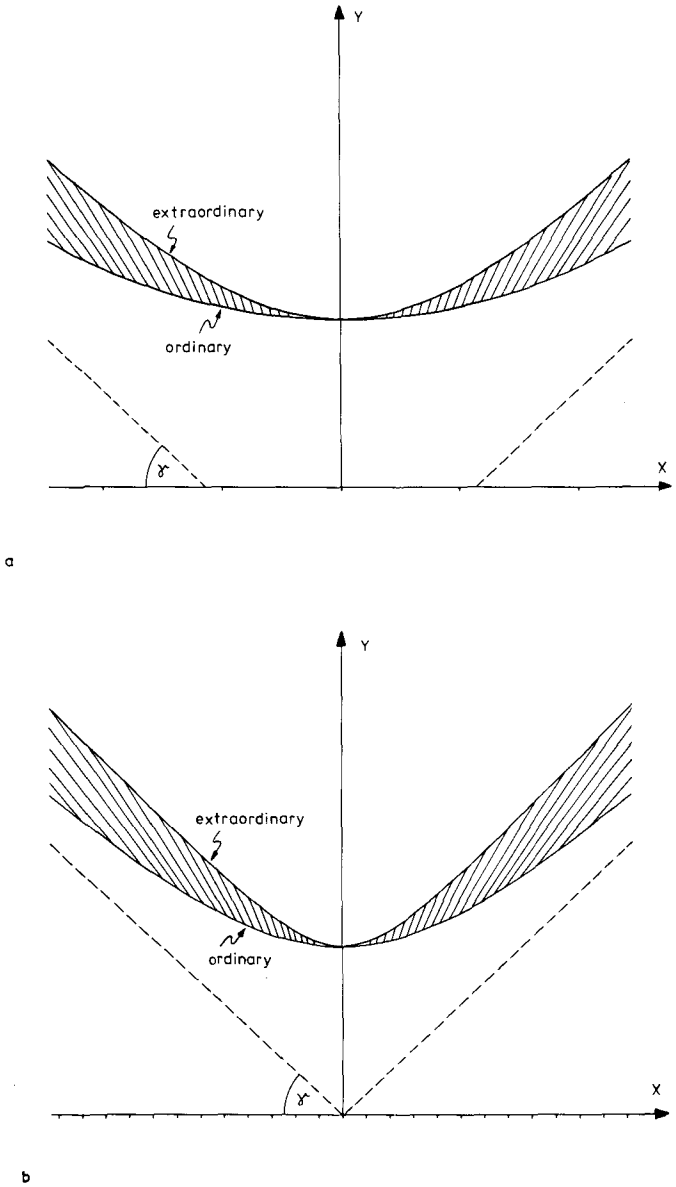

Figure 10. Relation between the ABOIF and ABEIF. The slanted lines between corresponding extraordinary and ordinary curves are the astigmatic image lines $\overline{IC}$ of object points placed along horizontal aerial lines. (a) $R/L=0.1$ (near-space). (b) $R/L=10$ (far-space). Same scales as in Fig. 8.

object point (arrangement with cylindrical symmetry). In this case the aerial visual field is the ABEIF (Fig. 9).

(v) When the eyes lie in a vertical plane, but not along a vertical line, the image of those aerial object points which lie in the vertical plane passing

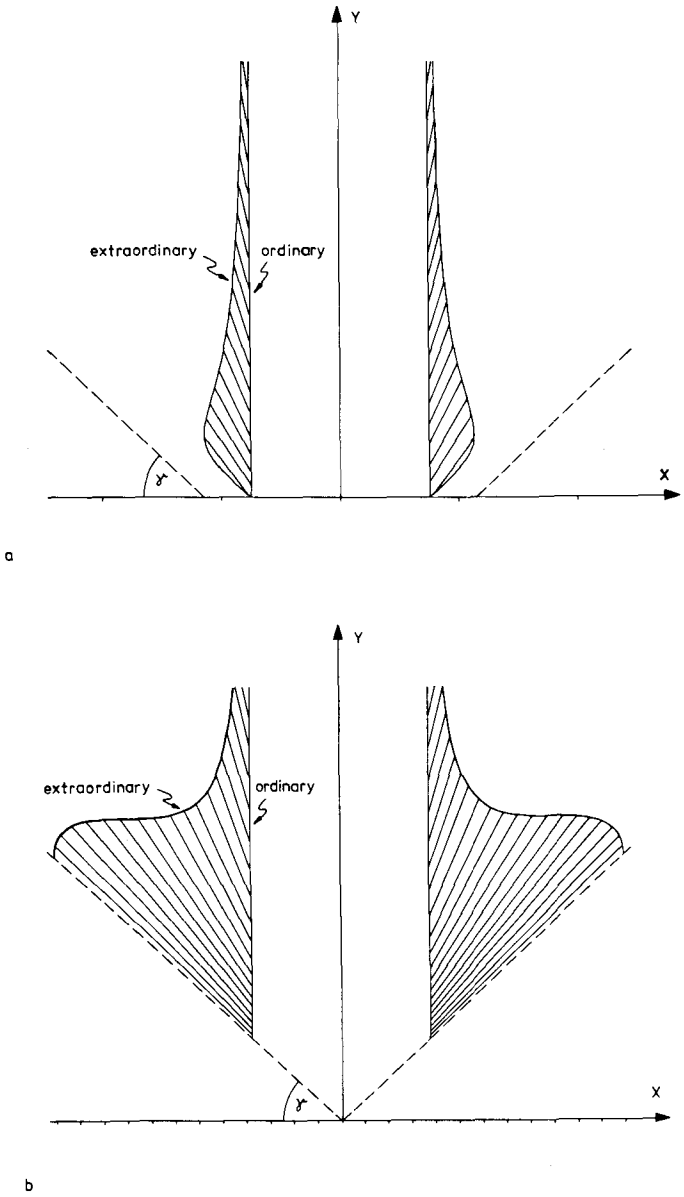

Figure 11. Same as Fig. 10 for object points placed along vertical aerial lines.

through the eyes appears in the ABEIF (Fig. 9). The aerial object points outside of this vertical plane have no binocular image point. In this case the aquatic animal cannot perceive the stereoscopic relationships.

(vi) When the eyes lie in a horizontal plane (parallel to the water surface), the image of the aerial object points which lie in the vertical plane involving the

eyes appears in the ABEIF (Fig. 9). The image of every other aerial object point appears in the ABOIF (Fig. 8). Hence the aerial visual field is predominantly the ABOIF, and it is the ABEIF only in the vertical plane involving the eyes.

The structures of the ABOIF and the ABEIF are significantly different (Figs 8 and 9). Those aquatic animals which must take into consideration the distorted structure of their aerial visual field in the visual detection of aerial prey or predator keep their eyes always in a horizontal plane. Maybe the undertaking to calculate the ABEIF (Fig. 9) is somewhat esoteric, however, the situation could arise when grazing fishes do turn around their long axis.

We thank Malcolm Carruthers for reading and correcting the manuscript. Financial support came from the Deutsche Forschungsgemeinschaft (SFB 307).

LITERATURE

Bekoff, M. and R. Dorr. 1976. *Bull. Psychonomical Soc.* **7**, 167–168.
Curio, E. 1976. *The Ethology of Predation.* Springer-Verlag: Berlin.
Dill, L. M. 1977. *Behavioral Ecology and Sociobiology* **2**, 169–184.
Harmon, R. and J. Cline. 1980. *Rod and Reel* **7**, 41–45.
Horváth, G. and D. Varjú. 1990. Geometric optical investigation of the underwater visual field of aerial animals. *Math. Biosci.*, in press.
Katzir, G. and N. Intrator. 1987. *J. Comparative Physiologie* **A160**, 517–523.
Lüling, K. H. 1963. *Sci. Am.* **209/1**, 100–108.
Schusterman, R. J. 1981. *The Psychological Record* **31**, 125–143.
Walker, J. 1984. *Sci. Am.* **250/3**, 108–113.

Received 30 May 1989
Revised 13 April 1990